An *in vivo* study of the impact of deficiency in the DNA repair proteins PAXX and XLF on development and maturation of the hemolymphoid system

Received for publication, September 3, 2019, and in revised form, January 3, 2020 Published, Papers in Press, January 8, 2020, DOI 10.1074/jbc.AC119.010924

Stefania Musilli[1], **Vincent Abramowski, Benoit Roch, and Jean-Pierre de Villartay**[2]

From the Laboratory of Genome Dynamics in the Immune System, Imagine Institute, INSERM UMR 1163, Université de Paris, 75015 Paris, France

Edited by Patrick Sung

Repair of DNA double-strand breaks by the nonhomologous end joining pathway is central for proper development of the adaptive immune system. This repair pathway involves eight factors, including XRCC4-like factor (XLF)/Cernunnos and the paralog of XRCC4 and XLF, PAXX nonhomologous end joining factor (PAXX). Xlf$^{-/-}$ and Paxx$^{-/-}$ mice are viable and exhibit only a mild immunophenotype. However, mice lacking both PAXX and XLF are embryonic lethal because postmitotic neurons undergo massive apoptosis in embryos. To decipher the roles of PAXX and XLF in both variable, diversity, and joining recombination and immunoglobulin class switch recombination, here, using Cre/lox-specific deletion to prevent double-KO embryonic lethality, we developed two mouse models of a conditional Xlf KO in a Paxx$^{-/-}$ background. Cre expressed under control of the iVav or CD21 promoter enabled Xlf deletion in early hematopoietic progenitors and splenic mature B cells, respectively. We demonstrate the XLF and PAXX interplay during variable, diversity, and joining recombination *in vivo* but not during class switch recombination, for which PAXX appeared to be fully dispensable. Xlf/Paxx double KO in hematopoietic progenitors resulted in a shorter lifespan associated with onset of thymic lymphomas, revealing a genome caretaking function of XLF/PAXX.

All living organisms have to face DNA damage, and particularly DNA double-strand breaks (DSBs),[3] which are considered the most toxic DNA lesions for cells and have either exogenous or endogenous origins (1). Development of the adaptive immune system early in life is a major source of programmed DSBs (prDSB), which are introduced by recombination-activating genes 1 and 2 (RAG1/2) during somatic DNA rearrangement (V(D)J recombination) of variable (V), diversity (D), and joining (J) elements of the T cell receptor and immunoglobulin genes in T and B cells in the thymus and bone marrow (BM), respectively (2, 3). In addition, immunoglobulin class switch recombination (CSR), which occurs during the terminal maturation of B lymphocytes in the spleen upon antigen triggering and results in exchange of the IgM constant region Cμ for a downstream C_H gene (γ, ϵ, or α) also proceeds through introduction of prDSBs by the activation-induced cytidine deaminase at switch regions (Sμ, Sγ, etc.) flanking C_H genes (4, 5).

The nonhomologous end joining (NHEJ) machinery is the DNA repair pathway that copes with these lymphoid-specific prDSBs. Briefly, the NHEJ machinery is composed of several factors, including Ku70/80, DNA PKCs, Artemis, DNA ligase IV, XRCC4, MRI, XLF, and PAXX, allowing recognition, processing, and religation of broken DNA ends (6, 7). Loss of function of many of these core factors leads to severe combined immunodeficiency in mice and humans because of arrest of B and T cell maturation as a result of abortive V(D)J recombination (8, 9). In the case of XRCC4 or ligase IV, it results in late embryonic lethality caused by massive apoptosis of postmitotic neurons (10–13). CSR is also affected to various extents by defective NHEJ (14, 15). XLF and PAXX appear to be an exception because their loss of function only marginally affects V(D)J recombination; Xlf or Paxx KO mice present with a mild immunophenotype characterized by a slightly reduced number of B and T lymphocytes (16–21). We and others identified functional relationships between XLF and other actors of V(D)J recombination that account for this peculiarity, such as ataxia telangiectasia-mutated (ATM) (22, 23) and the C terminus part of RAG2 (24). Indeed, Xlf/Atm or Xlf/Rag2^{cc} double-mutant mice lack B and T lymphocytes because of impaired V(D)J recombination (22, 24). The synthetic embryonic lethality between Paxx and Xlf also argues for a functional link between these two factors (19, 20). Although *Paxx*$^{-/-}$ mice do not present an overwhelming phenotype in general and in the immune system in particular, the increased sensitivity of Paxx-deficient cells to ionizing radiations in various settings corroborates implication of PAXX in DSB repair (19, 21, 25, 26). Moreover, E18.5 fetuses recovered from Xlf/Paxx double KO (DKO) mice revealed complete block of B and T cell development (19).

To better understand the role of PAXX in DSB repair during lymphocyte maturation and function and its interplay with Xlf in

This work was supported by grants from INSERM and the Institut National du Cancer (INCa PLBIO16-280) and by grants from La Ligue Nationale contre le Cancer (Equipe Labelisée LA LIGUE) and the AT-Europe Foundation. The authors declare that they have no conflicts of interest with the contents of this article.

[1] Supported by a fellowship from the AT-Europe Foundation.

[2] To whom correspondence should be addressed: INSERM UMR1163, Equipe Labellisée La Ligue, Institut Imagine, 24 bd. du Montparnasse, 75015 Paris, France. E-mail: devillartay@gmail.com.

[3] The abbreviations used are: DSB, double-strand break; prDSB, programmed double-strand break; V, variable; D, diversity; J, joining; BM, bone marrow; CSR, class switch recombination; NHEJ, nonhomologous end joining; DKO, double KO; CLP, common lymphoid progenitor; HSC, hematopoietic stem cell; LPS, lipopolysaccharide; ANOVA, analysis of variance; E18.5, embryonic day 18.5.

these processes in an *in vivo* setting, we developed two models of Xlf conditional KO in $Paxx^{-/-}$ mice to bypass the embryonic lethality of the DKO. Cre expression under the iVav and CD21 promoters allowed tissue-specific deletion of Xlf in hematopoietic precursors or only in splenic mature B cells, respectively.

Results

Generation of conditional Xlf KO in $Paxx^{-/-}$ mice

To analyze the combined role of PAXX and XLF during V(D)J recombination and CSR, we crossed $Paxx^{-/-}/Xlf^{-/flox}$ mice with transgenic mice expressing the Cre recombinase under the iVav and CD21 promoters, respectively. In the iVav model, Cre recombinase is first expressed in fetal liver and then in the bone marrow, spleen, thymus, and lymph nodes at postnatal stages (27), allowing specific deletion of *Xlf* in all hematopoietic lineages. In the ΔCD21 model, the Cre recombinase is expressed only in mature B lymphocytes (28), resulting in B cell–specific deletion of *Xlf*. For the two models, mice were born at a Mendelian ratio and did not present any morphological defects at birth, confirming bypass of the embryonic lethality seen in the constitutive Paxx/Xlf DKO. From this point on, the $Paxx^{-/-}Xlf^{-/fl}$iVav-Cre and $Paxx^{-/-}Xlf^{-/fl}$CD21-Cre models will be indicated as *Xlf*ΔiVav and *Xlf*ΔCD21, respectively. PCR analyses confirmed the effective deletion of Xlf in purified splenic mature B cells from *Xlf*ΔCD21 or BM from *Xlf*ΔiVav mice (Fig. 1, *A* and *B*). Xlf deletion in *Xlf*ΔCD21 B cells was further confirmed by Western blotting (Fig. 1*C*).

PAXX and XLF are redundant during VDJ recombination

DNA repair is a key mechanism for development of the immune system, and previous studies reported that mice with a single *Paxx* or *Xlf* deletion present overall normal B and T cell development (16–21). However, DKO of these factors leads to total blockage of the V(D)J recombination process both *in vitro* and *in vivo* (E18 recovered embryos), suggesting redundancy in their function (15, 19, 20, 29). Although only a slight but significant decrease in splenic and thymic cellularity was observed in $Xlf^{-/-}$ mice compared with $Paxx^{-/-}$ and WT mice (Fig. 1*D*), *Xlf*ΔiVav mice were lacking a visible thymus, and splenic cellularity was strongly diminished (Fig. 1*D*). Likewise, although flow cytometry analysis of T (CD4+ and CD8+) and B (IgM+/B220+) cells in either spleen or thymus revealed an indistinguishable phenotype in $Paxx^{-/-}$ and $Xlf^{-/-}$ mice compared with the WT (Fig. 1, *E* and *F*), *Xlf*ΔiVav mice presented a severe defect in both lymphoid populations. Moreover, BM from *Xlf*ΔiVav mice was also devoid of mature B cells and revealed arrest at the pre-proB cell stage (Fig. 1*E*). These results recapitulate the profound immune deficiency caused by a block in the V(D)J process noted previously in E18.5 *Paxx/Xlf* DKO fetuses (19), reinforcing the absolute requirement of the combined function of PAXX and XLF for proper development of the adaptive immune system.

PAXX is dispensable for CSR in vivo

We showed previously that loss of PAXX does not impair B cell development (19). The functional relationship between PAXX and XLF during late stages of B cell maturation was analyzed through CD21-Cre–mediated deletion of *Xlf* in $Paxx^{-/-}$ mature B cells (*Xlf*ΔCD21 mice). The overall development of both T and B cells was not affected in this setting (Fig. 1, *D–F*). Histological analysis of the spleen performed by hematoxylin and eosin staining revealed a conserved splenic architecture with the presence of germinal centers compared with WT or $Paxx^{-/-}$ mice, despite slightly decreased cellularity in $Xlf^{-/-}$ and *Xlf*ΔCD21 mice (Fig. 2*A*). We then analyzed the consequences of the concomitant *Paxx* and *Xlf* inactivation on CSR. CD43-negative sorted mature B cells from WT, $Paxx^{-/-}$, $Xlf^{-/-}$, and *Xlf*ΔCD21 mice were activated during 4 days *in vitro* to induce CSR toward the IgG1, IgG2b, or IgG3 isotypes. The B-cell proliferative capacity, as determined by Cell-Trace dilution, was not affected under any of the tested conditions (Fig. 2*B*). Although CSR to the three tested isotypes was not impaired in $Paxx^{-/-}$ B cells, as documented previously in CH12-B cells induced to switch to IgA *in vitro* (15), a significant decrease in the rate of switched cells toward all Ig isotypes was apparent for $Xlf^{-/-}$ B cells (Fig. 2, *C* and *D*), as reported previously (17). Interestingly, a similar CSR defect was observed in *Xlf*ΔCD21 B cells (Fig. 2, *C* and *D*). The absence of synthetic CSR dysfunction in *Xlf*ΔCD21 mice argues for the absence of PAXX contribution during CSR, at least quantitatively, even in the absence of XLF, as first noted *in vitro* (17).

PAXX and XLF participate in the maintenance of the lymphoid progenitor pool in the bone marrow

We then took advantage of *Xlf*ΔiVav mice to analyze the possible cooperation between PAXX and XLF for maintenance of the hemopoietic potential in these mice. We first measured the blood parameters in 7- to 10-week-old and 20- to 24-week-old mice. A shown in Fig. 3*A*, no differences were noticed in red blood cell and platelets counts for the various genotypes in the two age groups, indicating that myelopoiesis is not overtly affected by combined Paxx and Xlf deficiency. In contrast, a statistically significant decrease in total white blood cell and lymphocyte counts was observed in $Xlf^{-/-}$ mice, as described previously (16, 17), and in *Xlf*ΔiVav mice compared with $Paxx^{-/-}$ mice (Fig. 3*A*). Consistent with the major V(D)J recombination defect in *Xlf*ΔiVav mice described above, the decrease in lymphocyte numbers was more severe in *Xlf*ΔiVav animals than in Xlf simple KO animals. The rise in lymphocyte numbers in aged *Xlf*ΔiVav probably reflects lymphocyte homeostatic proliferation to some extent in aged mice. Analysis of bone marrow (Figs. 3, *B* and *C*) revealed that, although the total LSK pool was not altered in young and aged $Paxx^{-/-}$ and *Xlf*ΔiVav mice, the common lymphoid progenitor (CLP) pool was significantly decreased in young *Xlf*ΔiVav mice compared with $Paxx^{-/-}$ mice, with a concomitant increase in the short-term HSC pool (Fig. 3*C*). The variation of CLPs/short-term HSCs was further aggravated in aged mice. These results indicate a functional redundancy between PAXX and XLF at early stages during hematopoietic development, beyond the V(D)J recombination process.

The survival of mice is impaired by Xlf deletion in iVav-expressing cells

During a 1-year follow up, no difference in the survival of $Paxx^{-/-}$ and $Xlf^{-/-}$ mice was observed, which contrasted with

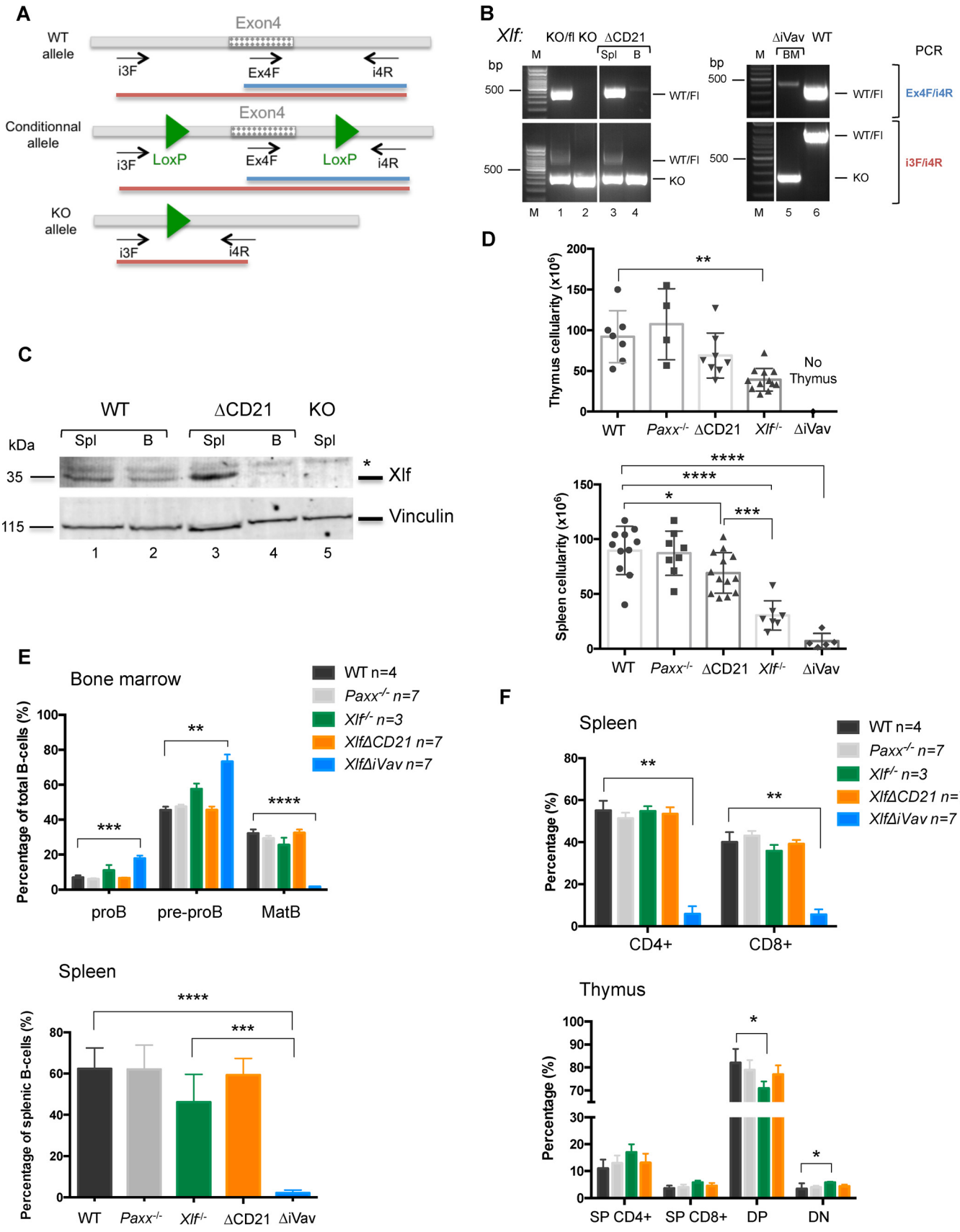
A
WT allele
Exon4
i3F
Ex4F
i4R
Conditionnal allele
LoxP
KO allele
B
Xlf:
KO/fl KO
ΔCD21
Spl
B
ΔiVav WT
BM
PCR
bp
500
WT/Fl
KO
Ex4F/i4R
i3F/i4R
M
1 2 3 4
5 6
C
WT
ΔCD21
KO
kDa
35
115
Xlf
Vinculin
1 2 3 4 5
D
Thymus cellularity (x10⁶)
No Thymus
Spleen cellularity (x10⁶)
WT
Paxx-/-
ΔCD21
Xlf-/-
ΔiVav
E
Bone marrow
WT n=4
Paxx-/- n=7
Xlf-/- n=3
XlfΔCD21 n=7
XlfΔiVav n=7
Percentage of total B-cells (%)
proB
pre-proB
MatB
Spleen
Percentage of splenic B-cells (%)
F
Spleen
Percentage (%)
CD4+
CD8+
Thymus
SP CD4+
SP CD8+
DP
DN

the sharply increased mortality of *Xlf*ΔiVav mice starting around 100 days (Fig. 4*A*). Aged *Xlf*ΔiVav mice showed decreased weight and moderate to severe alopecia (Fig. 4*B*). Moreover, three of five analyzed mice developed a thymic mass (Fig. 4*C*) whose histology revealed total loss of the thymus cortical and medullar architecture compared with the $Paxx^{-/-}$ thymus (Fig. 4*C*, *top panels*). Higher magnification revealed neoplastic cells with a large nucleus and dense cytoplasm, suggesting the tumorigenic nature of these cells (Fig. 4*C*, *bottom panels*, *arrowheads*). Thymic cell suspension analysis (Fig. 4*D*) showed a lack of activated T cells, indicated by negative TCRβ+ CD69+ staining and a shift in proliferative double-positive CD44+ CD62L+ cells for *Xlf*ΔiVav mice. These results are consistent with development of thymic lymphomas in aging *Xlf*ΔiVav mice, the possible cause of their accelerated death.

Discussion

We analyzed, for the first time *in vivo*, the PAXX and XLF interplay during V(D)J recombination and CSR through design of two conditional KO models: *Xlf*ΔiVav and *Xlf*ΔCD21. These two models circumvent the embryonic lethality resulting from combined lack of PAXX and XLF, as observed in previous studies (19, 20). *Xlf*ΔCD21 mice recapitulate the synthetic dysfunction of Paxx and Xlf in V(D)J recombination, manifested by the T−B−severe combined immunodeficiency phenotype. *Xlf*ΔCD21 mice confirmed the dispensability of PAXX in CSR, first proposed *in vitro* using the CH12 model (15), as shown by the absence of an additive effect of Paxx deficiency over Xlf KO alone. Overall, these results are in line with previous studies and suggest the existence of two distinct mechanisms for repair of programmed DNA breaks induced during V(D)J and CSR. They suggest that, in contrast to what happens during V(D)J recombination, XLF and PAXX do not complement each other for DNA end synapsis during CSR, in line with recent findings *in vitro*, proposing that Ku and XRCC4/DNA-Lig4 can initiate synapse formation on their own without the combined contribution of PAXX and XLF, at least on blunt DNA ends (30). Likewise, PAXX failed to rescue the defect in precise DNA end joining resulting from Xlf deficiency in a CRISPR/Cas9 model of DNA repair (31). It is thus proposed that classical NHEJ factors such as XLF or PAXX are involved in precise (without indels) DNA blunt end ligation but that their redundancy may vary depending on the DSB context. In that respect, it is worth mentioning that DSBs that occur during CSR are very unique, as they occur within large regions of repetitive sequences (called S for switch regions).

Last, the conditional *Xlf*ΔiVav model enabled analysis of the impact of Paxx/Xlf deficiency on the hematopoietic potential of aging mice, which was not possible with models used in previously published studies. For the first time, we could observe a shortened lifespan and the appearance of spontaneous thymic lymphomas without the need of a tumor accelerator background such as TP53 KO in *Xlf*ΔiVav aged mice, suggesting an additional role of PAXX/XLF as a genome caretaker in the context of RAG1/2-induced breaks because those thymic lymphomas were not observed in aged *Xlf*ΔCD21 mice. Although new studies are needed for full characterization of these hemopathies, we suggest the possible implication of aberrant oncogenic rearrangements to explain their appearance, given the previous demonstration of chromosomal translocations followed by production of fusion oncogenic genes in mouse cells in the context of classical NHEJ factor deficiencies (24, 32–35).

Materials and methods

Generation of conditional Xlf KO mice on a PAXX KO background

C57/Bl6 $Paxx^{-/-}Xlf^{+/-}$-CD21-cre or $Paxx^{-/-}Xlf^{+/-}$-iVav-cre mice were intercrossed with $Paxx^{-/-}Xlf^{flox/flox}$ mice to generate $Paxx^{-/-}Xlf-/^{flox}$CD21-cre or $Paxx^{-/-}Xlf^{-/flox}$iVav-cre mice and to specifically delete the *Xlf* gene under the expression of Cre recombinase along with the CD21 or iVav promoters. All mice used for this work were 7–10 weeks old (considered young mice) or 20–24 weeks old (considered old mice), kept under pathogen-free conditions, and sacrificed humanely. Mouse experiments were performed with approval from the local ethics committee and the French Ministry of Education and Research.

Mice were genotyped for *Paxx*, *Xlf*, *CD21*-cre, *iVav*-cre, and *Xlf*-flox by PCR on tail DNA. Exon 4 deletion of *Xlf* was analyzed as described previously (16) using the following primers: i4R (5′-GTCCCCAGCTGTTAAGAGTTTC-3′), i3F (5′-CTATGGAAGCCAGGAGAGAATG-3′), and Ex4F (5′-GGATGAAGGACCTTGAGATCC-3′). Under the PCR conditions used, the i3F/i4R combination of primers allowed detection of the KO allele (445 bp) but not of the WT or flox alleles because of the large PCR size (1.2–1.4 kb). The WT and flox alleles were identified using the Ex4F/i4R (438 bp) combination, which did not amplify the KO allele. Expression of XLF was analyzed by Western blotting on splenic protein extracts using a rabbit polyclonal anti-XLF antibody (A300-730A, Bethyl Laboratories). *Paxx* genotyping was performed as described previously (19) using the following primer pair: MuPAXX_F1, 5′-CAACCTTGAGTACCGCCCAT-3; MuPAXX_R1, 5′-CAACCTTGAGTACCGCCCAT-3′.

Figure 1. Xlf conditional KO validation and redundancy of PAXX and XLF for V(D)J. *A*, design of primers for specific detection of the various *Xlf* alleles. WT and Flox alleles were identified by PCR using Ex4F/i4R combination. The *Xlf* KO allele was revealed by shortening of the i3F/i4R PCR products (445 bp) as a consequence of exon 4 deletion. *B*, genotyping of the various Xlf alleles. Although both WT/Flox and KO alleles were present in the total spleen of *Xlf*ΔCD21 mice (*Spl*, *lane 4*), only the KO allele was revealed in purified B lymphocytes (*B*, *lane 5*) from these mice, attesting to efficient and restricted Cre-mediated deletion in B cells. Likewise, only the KO allele was identified (except for a light nonspecific product) in BM from *Xlf*ΔiVav mice. Panels are from different gels. *M*, molecular wheight marker. *C*, Western blot analysis of XLF deletion in mature splenic B cells (*lane 4*) from *Xlf*ΔCD21 and total spleen from $Xlf^{-/-}$ mice (*lane 5*). *Asterisk*, nonspecific band. Vinculin was included as a loading control. *D*, spleen and thymus cellularity in WT, $Paxx^{-/-}$, $Xlf^{-/-}$, *Xlf*ΔCD21, and *Xlf*ΔiVav mice. Results are represented as the mean ± S.E. *E*, quantification of T cells in the spleen and thymus based on CD4/CD8 staining in CD3+ populations. Results are represented as the mean ± S.E. *SP*, single-positive; *DP*, double-positive; *DN*, double-negative. *F*, quantification of B cells in the BM and spleen based on IgM/B220 staining of total B cells for BM and in the CD3− splenic population. ProB cells in BM are quantified based on CD43 staining within the pre-proB population. Results are represented as the mean ± S.E. *MatB*, mature B cells. All statistical analyses were performed using one-way ANOVA, and significant differences are indicated as follows: *, $p < 0.05$; **, $p < 0.01$; ***, $p < 0.001$; ****, $p < 0.0001$; *ns*, not significant.

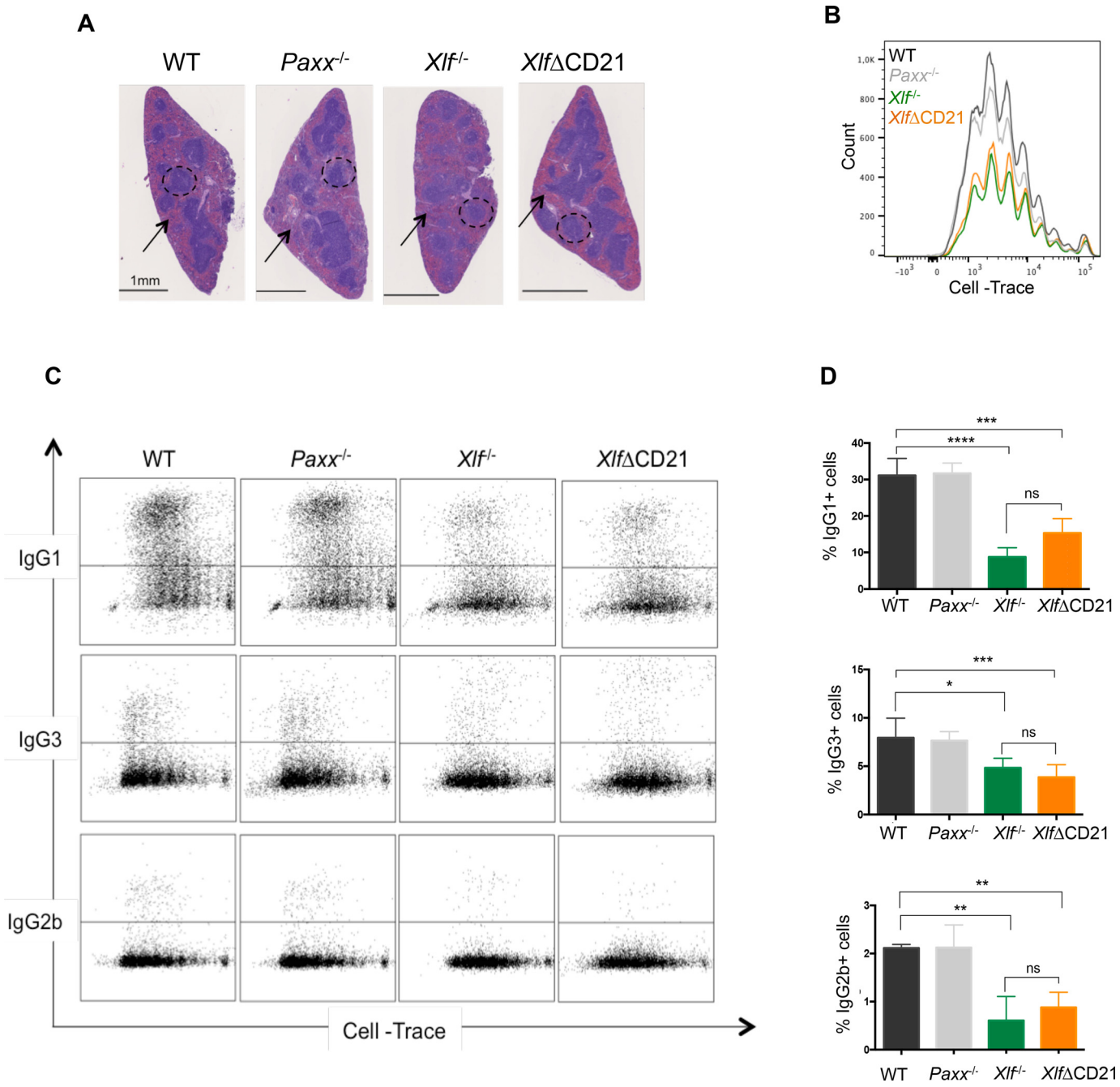

Figure 2. PAXX is dispensable for CSR *in vivo*. *A*, spleen sections of WT, *Paxx*$^{-/-}$, *Xlf*$^{-/-}$, and *Xlf*ΔCD21 mice stained with hematoxylin and eosin. Germinal centers are indicated by *dotted circles* and red blood cell areas by *arrows*. *Scale bars* = 1 mm. *B*, representative flow cytometry analysis of WT, *Paxx*$^{-/-}$, *Xlf*$^{-/-}$, and *Xlf*ΔCD21 B cell proliferation after 4 days of stimulation in specific medium for the switch toward IgG1, IgG3, and IgG2b isotypes, based on Cell-Trace dilution. *C*, representative flow cytometry plots of CD43− mature B cells switched toward IgG1, IgG3, or IgG2b isotypes, based on Cell-Trace dilution and isotype staining in WT, *Paxx*$^{-/-}$, *Xlf*$^{-/-}$, and *Xlf*ΔCD21 mice. *D*, quantification of IgG1-, IgG3-, and IgG2b-switched mature CD43− B cells in WT, *Paxx*$^{-/-}$, *Xlf*$^{-/-}$, and *Xlf*ΔCD21 mice after 4 days of stimulation in LPS or LPS/IL-4–supplemented medium, based on the Cell-Trace dilution and isotype staining. Results are represented as the mean of four independent experiments ± S.E. All statistical analyses were performed using one-way ANOVA, and significant differences are indicated as follows: *, $p < 0.05$; **, $p < 0.01$; ***, $p < 0.001$; ****, $p < 0.0001$; *ns*, not significant.

Flow cytometry analysis

For the immunophenotype, the thymus, spleen and bone marrow were harvested. Thymic populations were identified by anti-CD8 and anti-CD4, and the double negative population was stained with anti-CD44 and anti-CD25 mouse antibodies (all from Sony Biotechnologies). Thymic lymphomas were additionally stained with anti-CD69, anti-CD62L, and anti-TCRβ. Splenic T cells were stained with anti-CD3, anti-CD4, and anti-CD8, whereas B cells were identified by anti-B220 and anti-IgM (all from Sony Biotechnologies). Bone marrow was obtained from one femur and stained with anti-IgM, anti-B220, and anti-CD43 (all from Sony Biotechnologies). Flow cytometry was performed on a BD-LSR Fortessa (BD Biosciences).

For the study of hematopoietic stem cells, bone marrow was stained with Lin$^-$ antibody mixture (BD Biosciences), anti-c-kit, anti-CD34, anti-Sca1, anti-Flt3, and anti-Il7ra (mouse anti-

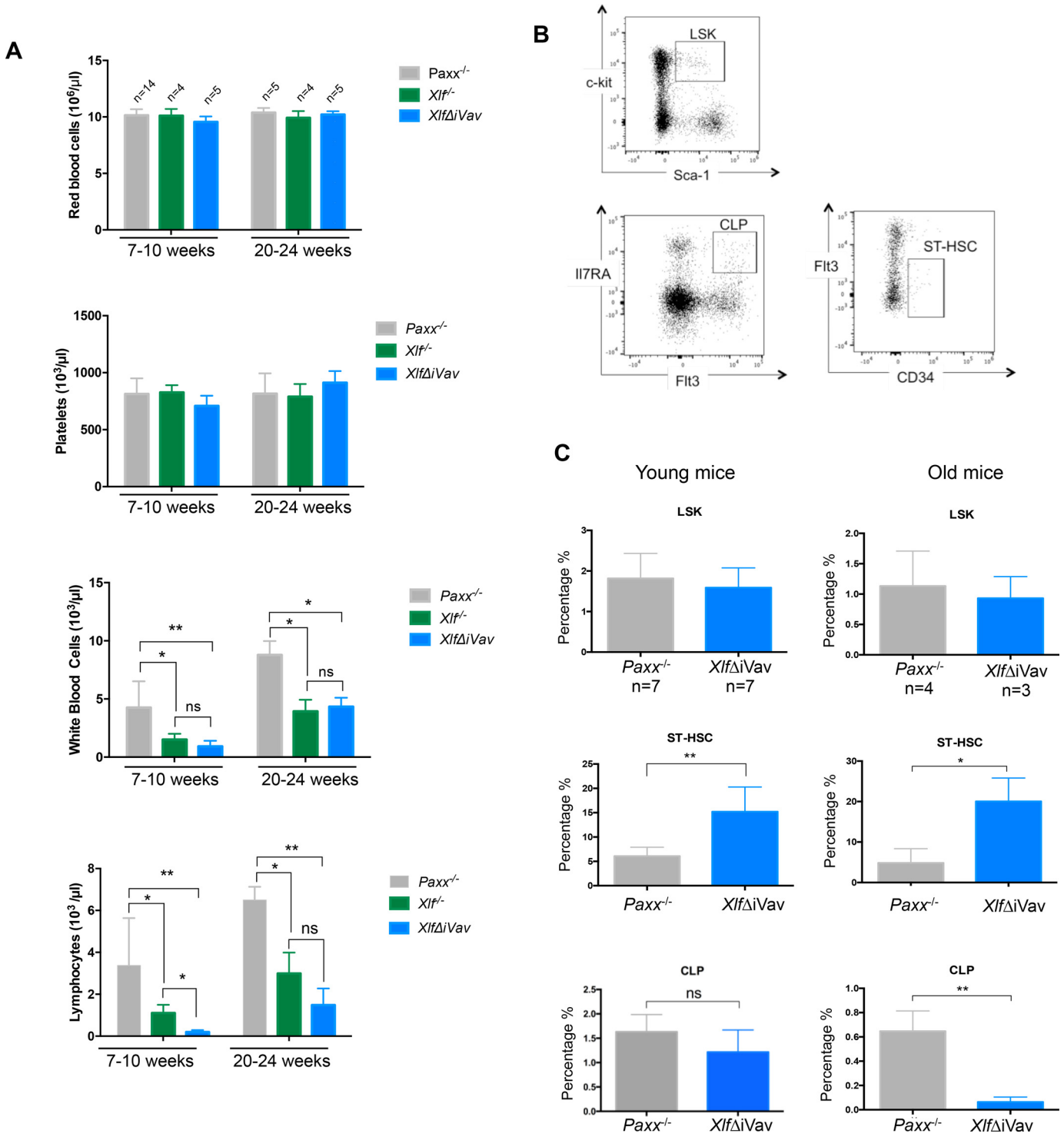

Figure 3. Paxx/Xlf deletion in bone marrow impairs lymphoid progenitors. *A*, quantification of red blood cell, platelet, white blood cell, and lymphocyte concentrations in the blood of 7- to 10-week-old and 20- to 24-week-old *Paxx*$^{-/-}$, *Xlf*$^{-/-}$, and *Xlf*ΔiVav mice. Results are indicated as mean ± S.E. Statistical analyses were performed by one-way ANOVA. Significant differences are indicated as follows: *, $p < 0.05$; **, $p < 0.01$; *ns*, not significant. *B*, gating strategy for analysis of hematopoietic populations in BM. Analysis were performed in a Lin− population based on staining with c-kit, Sca-1, Flt3, CD34, and IL7RA antibodies for assessment of Lin−c-kit+Sca−1+ cells (LSK), short-term (*ST*) hematopoietic stem cells HSCs, and CLPs. *C*, quantification of flow cytometry analyses for the hematopoietic compartment of 7- to 10-week old (*young*) and 20- to 24-week-old (*old*) *Paxx*$^{-/-}$ and *Xlf*ΔiVav mice. The percentages of total LSK, short-term HSC, and CLP populations are represented as mean ± S.E., and statistical analyses were performed by Student's *t* test. Significant differences are indicated as follows: *, $p < 0.05$; **, $p < 0.01$.

bodies, all from Sony Biotechnologies). Flow cytometry was performed on a Sony SP6800 Spectral analyzer. All flow cytometry analyses and quantifications were performed on FlowJo software

Blood measurement

Blood from mice was collected by intracardiac puncture after anesthesia by injection of a mixture of ketamine and xylazine.

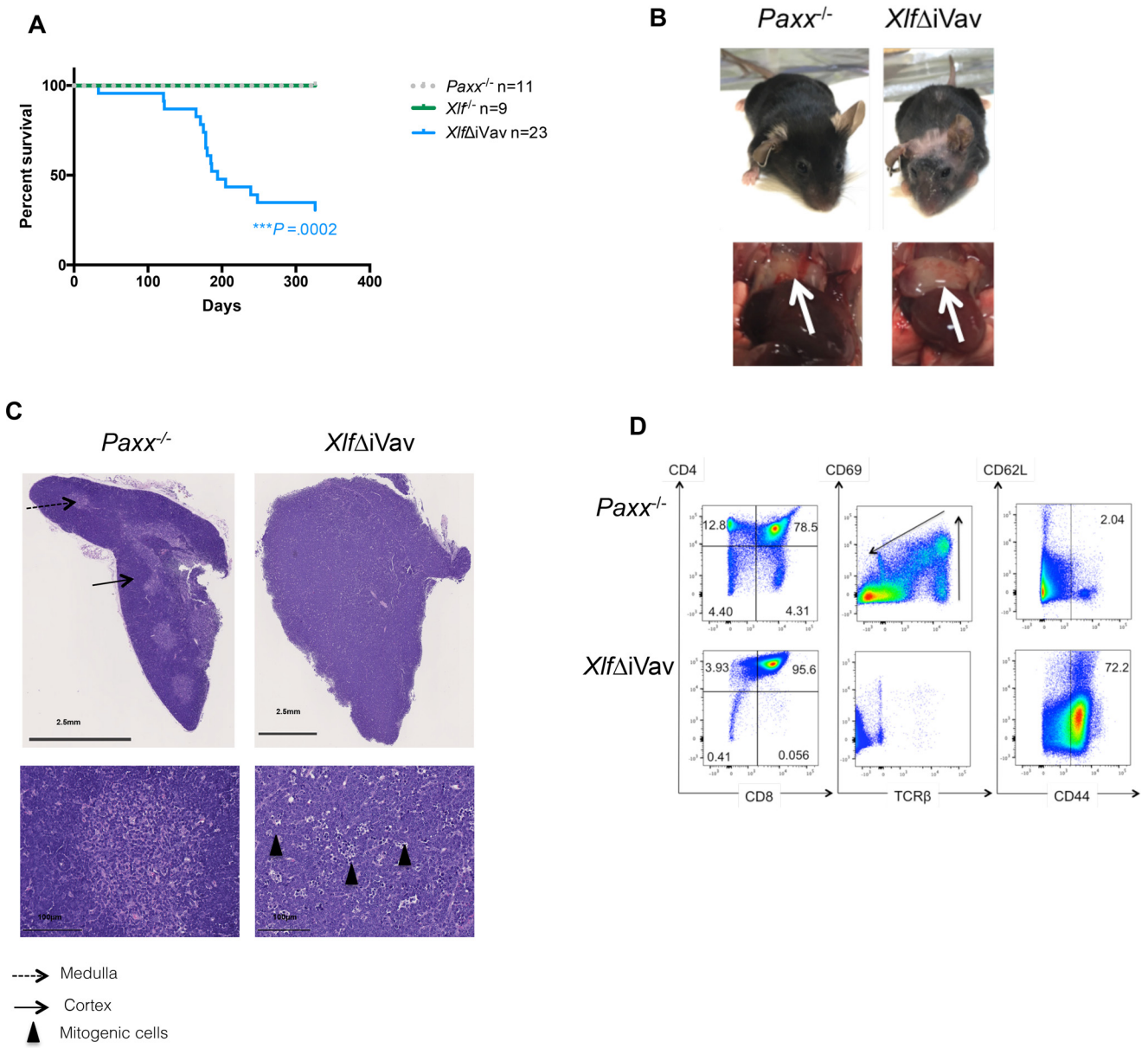

Figure 4. Cooperation between PAXX and XLF for mouse survival and prevention of thymic lymphomas. *A*, survival curve after 1 year of follow-up of *Paxx*$^{-/-}$, *Xlf*$^{-/-}$, and *Xlf*ΔiVav mice. Statistical analyses were performed by Kaplan–Meyer χ^2 test, and significant differences are represented as follows: ***, $p = 0.0002$. *B*, representative picture of one *Paxx*$^{-/-}$ and one *Xlf*ΔiVav mouse at 20 weeks. The thymus in the *Paxx*$^{-/-}$ mouse and the thymic mass in the *Xlf*ΔiVav mouse are indicated by *arrows*. *C*, representative H&E staining of *Paxx*$^{-/-}$ thymus and *Xlf*ΔiVav thymic lymphoma sections (*top panels*) and at higher magnification (*bottom panels*). The cortical structure is indicated by the *solid arrow* and the medulla by the *dotted arrow*. *Arrowheads* indicate neoplastic cells observed at higher magnification. *Scale bars* = 2.5 mm (*top panels*) and 100 μm (*bottom panels*). *D*, representative flow cytometry analyses for the thymus of the *Paxx*$^{-/-}$ mouse and the thymic lymphoma of the *Xlf*ΔiVav mouse. Analyses were performed on viable cells (negative Sytox staining), and the gates were defined by the indicated antibodies. The percentages for each population are indicated in the quadrants.

Blood was then analyzed on a Procyte Dx Hematology analyzer (IDEXX Bioanalytics).

Histological analysis

The thymus and spleen were harvested, fixed overnight in 4% paraformaldehyde, washed with PBS, paraffin-embedded, and sectioned at 4-μm thickness. Sections were then stained with hematoxylin and eosin for morphological analysis.

Purification and activation of splenic mature B cells in vitro

Mature B cells were negatively sorted from the spleen using CD43+ magnetic beads following the manufacturer's instructions (Miltenyi). The negative fraction containing CD43− mature B cells was harvested and labeled with Cell-Trace (Thermo Fisher). For each condition, 500 000 cells were plated in triplicate in a 6-well plate in Iscove's modified Dulbecco's medium+ Glutamax medium supplemented with 10% fetal bovine serum, 1% penicillin–streptomycin, 1% sodium pyruvate, 1% HEPES, 1% nonessential amino acids, and 0.1% β-mercaptoethanol (all from Thermo Fisher). Cells were incubated for 4 days with 25 μg/ml LPS from *Escherichia coli* (Sigma) + 20 ng/ml IL-4 (R&D Systems) for IgG1 switching or with 25 μg/ml LPS for IgG3 and IgG2b switching. At the end of incubation, cells were collected and labeled with anti-mouse B220-PE

(Sony Biotechnologies) and anti-mouse biotin-coupled IgG1, IgG2b, and IgG3 (R&D Systems), followed by incubation with allophycocyanin–streptavidin (Thermo Fisher). Cells were analyzed on a BD LSR-Fortessa (BD Bioscience).

Statistics

All statistics were determined using Prism (GraphPad Software). Groups were analyzed by one-way ANOVA or Student's *t* test as indicated, and the difference was considered statistically significant at $p < 0.05$.

Author contributions—S. M. and V. A. data curation; S. M., V. A., and B. R. formal analysis; S. M. and V. A. investigation; S. M. and J.-P. d. V. writing-original draft; J.-P. d. V. conceptualization; J.-P. d. V. supervision.

Acknowledgments—We thank Jérémy Paumier (Centre de Développement des Technologies Avancées, Orléans, France) for taking care of the mouse lines and Sophie Berissi for help with histological analyses.

References

1. Betermier, M., Borde, V., and Villartay, J. P. (2019) Coupling DNA damage and repair: an essential safeguard during programmed DNA double-strand breaks? *Trends Cell Biol.* **30,** 87–96 CrossRef Medline
2. Bassing, C. H., Swat, W., and Alt, F. W. (2002) The mechanism and regulation of chromosomal V(D)J recombination. *Cell* **109,** S45–S55 CrossRef Medline
3. Arya, R., and Bassing, C. H. (2017) V(D)J Recombination exploits DNA damage responses to promote immunity. *Trends Genet.* **33,** 479–489 CrossRef Medline
4. Chaudhuri, J., Basu, U., Zarrin, A., Yan, C., Franco, S., Perlot, T., Vuong, B., Wang, J., Phan, R. T., Datta, A., Manis, J., and Alt, F. W. (2007) Evolution of the immunoglobulin heavy chain class switch recombination mechanism. *Adv. Immunol.* **94,** 157–214 CrossRef Medline
5. Methot, S. P., and Di Noia, J. M. (2017) Molecular mechanisms of somatic hypermutation and class switch recombination. *Adv. Immunol.* **133,** 37–87 CrossRef Medline
6. Hung, P. J., Johnson, B., Chen, B. R., Byrum, A. K., Bredemeyer, A. L., Yewdell, W. T., Johnson, T. E., Lee, B. J., Deivasigamani, S., Hindi, I., Amatya, P., Gross, M. L., Paull, T. T., Pisapia, D. J., Chaudhuri, J., *et al.* (2018) MRI is a DNA damage response adaptor during classical non-homologous end joining. *Mol. Cell* **71,** 332–342.e8 CrossRef Medline
7. Chang, H. H. Y., Pannunzio, N. R., Adachi, N., and Lieber, M. R. (2017) Non-homologous DNA end joining and alternative pathways to double-strand break repair. *Nat. Rev. Mol. Cell Biol.* **18,** 495–506 CrossRef Medline
8. de Villartay, J. P., Fischer, A., and Durandy, A. (2003) The mechanisms of immune diversification and their disorders. *Nat. Rev. Immunol.* **3,** 962–972 CrossRef Medline
9. de Villartay, J. P. (2015) Congenital defects in V(D)J recombination. *Br. Med. Bull.* **114,** 157–167 CrossRef Medline
10. Soulas-Sprauel, P., Le Guyader, G., Rivera-Munoz, P., Abramowski, V., Olivier-Martin, C., Goujet-Zalc, C., Charneau, P., and de Villartay, J. P. (2007) Role for DNA repair factor XRCC4 in immunoglobulin class switch recombination. *J. Exp. Med.* **204,** 1717–1727 CrossRef Medline
11. Gao, Y., Sun, Y., Frank, K. M., Dikkes, P., Fujiwara, Y., Seidl, K. J., Sekiguchi, J. M., Rathbun, G. A., Swat, W., Wang, J., Bronson, R. T., Malynn, B. A., Bryans, M., Zhu, C., Chaudhuri, J., *et al.* (1998) A critical role for DNA end-joining proteins in both lymphogenesis and neurogenesis. *Cell* **95,** 891–902 CrossRef Medline
12. Barnes, D. E., Stamp, G., Rosewell, I., Denzel, A., and Lindahl, T. (1998) Targeted disruption of the gene encoding DNA ligase IV leads to lethality in embryonic mice. *Curr. Biol.* **8,** 1395–1398 CrossRef Medline
13. Frank, K. M., Sekiguchi, J. M., Seidl, K. J., Swat, W., Rathbun, G. A., Cheng, H. L., Davidson, L., Kangaloo, L., and Alt, F. W. (1998) Late embryonic lethality and impaired V(D)J recombination in mice lacking DNA ligase IV. *Nature* **396,** 173–177 CrossRef Medline
14. Han, L., and Yu, K. (2008) Altered kinetics of nonhomologous end joining and class switch recombination in ligase IV-deficient B cells. *J. Exp. Med.* **205,** 2745–2753 CrossRef Medline
15. Kumar, V., Alt, F. W., and Frock, R. L. (2016) PAXX and XLF DNA repair factors are functionally redundant in joining DNA breaks in a G_1-arrested progenitor B-cell line. *Proc. Natl. Acad. Sci. U.S.A.* **113,** 10619–10624 CrossRef Medline
16. Vera, G., Rivera-Munoz, P., Abramowski, V., Malivert, L., Lim, A., Bole-Feysot, C., Martin, C., Florkin, B., Latour, S., Revy, P., and de Villartay, J. P. (2013) Cernunnos deficiency reduces thymocyte life span and alters the T cell repertoire in mice and humans. *Mol. Cell Biol.* **33,** 701–711 CrossRef Medline
17. Li, G., Alt, F. W., Cheng, H. L., Brush, J. W., Goff, P. H., Murphy, M. M., Franco, S., Zhang, Y., and Zha, S. (2008) Lymphocyte-specific compensation for XLF/cernunnos end-joining functions in V(D)J recombination. *Mol. Cell* **31,** 631–640 CrossRef Medline
18. Roch, B., Abramowski, V., Chaumeil, J., and de Villartay, J. P. (2019) Cernunnos/Xlf deficiency results in suboptimal V(D)J recombination and impaired lymphoid development in mice. *Front. Immunol.* **10,** 443 CrossRef Medline
19. Abramowski, V., Etienne, O., Elsaid, R., Yang, J., Berland, A., Kermasson, L., Roch, B., Musilli, S., Moussu, J. P., Lipson-Ruffert, K., Revy, P., Cumano, A., Boussin, F. D., and de Villartay, J. P. (2018) PAXX and Xlf interplay revealed by impaired CNS development and immunodeficiency of double KO mice. *Cell Death Differ.* **25,** 444–452 CrossRef Medline
20. Balmus, G., Barros, A. C., Wijnhoven, P. W., Lescale, C., Hasse, H. L., Boroviak, K., le Sage, C., Doe, B., Speak, A. O., Galli, A., Jacobsen, M., Deriano, L., Adams, D. J., Blackford, A. N., and Jackson, S. P. (2016) Synthetic lethality between PAXX and XLF in mammalian development. *Genes Dev.* **30,** 2152–2157 CrossRef Medline
21. Gago-Fuentes, R., Xing, M., Sæterstad, S., Sarno, A., Dewan, A., Beck, C., Bradamante, S., Bjørås, M., and Oksenych, V. (2018) Normal development of mice lacking PAXX, the paralogue of XRCC4 and XLF. *FEBS Open Bio.* **8,** 426–434 CrossRef Medline
22. Zha, S., Guo, C., Boboila, C., Oksenych, V., Cheng, H. L., Zhang, Y., Wesemann, D. R., Yuen, G., Patel, H., Goff, P. H., Dubois, R. L., and Alt, F. W. (2011) ATM damage response and XLF repair factor are functionally redundant in joining DNA breaks. *Nature* **469,** 250–254 CrossRef Medline
23. Kumar, V., Alt, F. W., and Oksenych, V. (2014) Functional overlaps between XLF and the ATM-dependent DNA double strand break response. *DNA Repair* **16,** 11–22 CrossRef Medline
24. Lescale, C., Abramowski, V., Bedora-Faure, M., Murigneux, V., Vera, G., Roth, D. B., Revy, P., de Villartay, J. P., and Deriano, L. (2016) RAG2 and XLF/Cernunnos interplay reveals a novel role for the RAG complex in DNA repair. *Nat. Commun.* **7,** 10529 CrossRef Medline
25. Hung, P. J., Chen, B. R., George, R., Liberman, C., Morales, A. J., Colon-Ortiz, P., Tyler, J. K., Sleckman, B. P., and Bredemeyer, A. L. (2017) Deficiency of XLF and PAXX prevents DNA double-strand break repair by non-homologous end joining in lymphocytes. *Cell Cycle* **16,** 286–295 CrossRef Medline
26. Dewan, A., Xing, M., Lundbæk, M. B., Gago-Fuentes, R., Beck, C., Aas, P. A., Liabakk, N. B., Saeterstad, S., Chau, K. T. P., Kavli, B. M., and Oksenych, V. (2018) Robust DNA repair in PAXX-deficient mammalian cells. *FEBS Open Bio.* **8,** 442–448 CrossRef Medline
27. Bustelo, X. R., Rubin, S. D., Suen, K. L., Carrasco, D., and Barbacid, M. (1993) Developmental expression of the vav protooncogene. *Cell Growth Differ.* **4,** 297–308 Medline
28. Takahashi, K., Kozono, Y., Waldschmidt, T. J., Berthiaume, D., Quigg, R. J., Baron, A., and Holers, V. M. (1997) Mouse complement receptors type 1 (CR1;CD35) and type 2 (CR2;CD21): expression on normal B cell subpopulations and decreased levels during the development of autoimmunity in MRL/lpr mice. *J. Immunol.* **159,** 1557–1569 Medline
29. Lescale, C., Lenden Hasse, H., Blackford, A. N., Balmus, G., Bianchi, J. J., Yu, W., Bacoccina, L., Jarade, A., Clouin, C., Sivapalan, R., Reina-San-Martin, B., Jackson, S. P., and Deriano, L. (2016) Specific roles of XRCC4

paralogs PAXX and XLF during (1)V(D)J recombination. *Cell Rep.* **16,** 2967–2979 CrossRef Medline

30. Zhao, B., Watanabe, G., Morten, M. J., Reid, D. A., Rothenberg, E., and Lieber, M. R. (2019) The essential elements for the noncovalent association of two DNA ends during NHEJ synapsis. *Nat. Commun.* **10,** 3588 CrossRef Medline
31. Bhargava, R., Sandhu, M., Muk, S., Lee, G., Vaidehi, N., and Stark, J. M. (2018) C-NHEJ without indels is robust and requires synergistic function of distinct XLF domains. *Nat. Commun.* **9,** 2484 CrossRef Medline
32. Zha, S., Bassing, C. H., Sanda, T., Brush, J. W., Patel, H., Goff, P. H., Murphy, M. M., Tepsuporn, S., Gatti, R. A., Look, A. T., and Alt, F. W. (2010) ATM-deficient thymic lymphoma is associated with aberrant tcrd rearrangement and gene amplification. *J. Exp. Med.* **207,** 1369–1380 CrossRef Medline
33. Deriano, L., Chaumeil, J., Coussens, M., Multani, A., Chou, Y., Alekseyenko, A. V., Chang, S., Skok, J. A., and Roth, D. B. (2011) The RAG2 C terminus suppresses genomic instability and lymphomagenesis. *Nature* **471,** 119–123 CrossRef Medline
34. Boboila, C., Alt, F. W., and Schwer, B. (2012) Classical and alternative end-joining pathways for repair of lymphocyte-specific and general DNA double-strand breaks. *Adv. Immunol.* **116,** 1–49 CrossRef Medline
35. Bunting, S. F., and Nussenzweig, A. (2013) End-joining, translocations and cancer. *Nat. Rev. Cancer* **13,** 443–454 CrossRef Medline